PERGAMON

International Journal of Heat and Mass Transfer 42 (1999) 1389–1403

International Journal of HEAT and MASS TRANSFER

Near-wall hydrodynamics in a scale-model circulating fluidized bed

Peter D. Noymer[1], Leon R. Glicksman*

Department of Mechanical Engineering, Massachusetts Institute of Technology, Cambridge, MA 02139, U.S.A.

Received 16 February 1998; in final form 27 July 1998

Abstract

The motion of clusters of particles at the wall of a circulating fluidized-bed (CFB) has been observed using a thermal-imaging technique for flow visualization. Dynamic properties of clusters adjacent to the wall were measured, including the residence time of the clusters at the wall and the velocities at which they travel. The properties were measured for variations in superficial gas velocity, external solids recirculation rate, density of the solid material, and average particle diameter. Average cluster velocities were measured in the range of 1.1–1.2 m s^{-1}, with little dependence seen on any of the operating conditions. Average cluster–wall contact times were measured in the range of 0.15–0.50 s, with some dependence on solid density observed.

A simplified model for the motion of clusters near a wall has been developed, treating the clusters as permeable bodies traveling adjacent to a wall in a quiescent fluid. This model allows for the application of computational methods to study the flow in and around clusters, as well as the calculation of lift (normal to the wall) and drag (parallel to the wall) forces on the clusters. These simulations show the presence of a substantial drag force, which helps explain the magnitudes of the observed cluster velocities. The simulations also show the presence of a lift force, which can be used to predict the observed cluster–wall contact times. The agreement between the simulations and the measured contact times is an indication that the lifting force is the phenomenon governing the removal or shedding of clusters from the wall region.

Nomenclature

A area
c specific heat capacity
c_d drag coefficient
c_l lift, drag coefficient
d_p mean particle diameter
D diameter
D_{cl} cluster diameter
f fraction of wall covered by clusters
F lift, drag force
g acceleration due to gravity
G_s solid recirculation rate
h heat-transfer coefficient
h_{conv} total bed-to-wall convective heat transfer coefficient
h_{gas} gas-phase heat transfer coefficient
k thermal conductivity
L riser height
m_{cl} cluster mass
P pressure
R thermal resistance
Re Reynolds number
t contact time between cluster and wall
T bed temperature
u velocity
u_{cl} cluster velocity
u_{mf} minimum fluidization velocity
u_0 gas superficial velocity
v velocity
x axial position of cluster
x' axial velocity of cluster
x'' axial acceleration of cluster

* Corresponding author. Tel.: 001 617 253 2233; fax: 001 617 258 7817; e-mail: glicks@mit.edu

[1] Present address: Department of Mechanical Engineering, Carnegie Mellon University, Pittsburgh, PA 15213, U.S.A.

0017–9310/98/$ - see front matter
PII: S0017–9310(98)00238–5

y lateral position of cluster
y' lateral velocity of cluster
y'' lateral acceleration of cluster
y_* dimensionless cluster–wall gap.

Greek symbols
ε_{cl} cluster void fraction
κ permeability
μ dynamic viscosity
ρ density
ρ_g gas density
ρ_s solid density
ρ_* solid–gas density ratio.

1. Introduction

A circulating fluidized bed (CFB) is a gas–solid flow reactor in which the net flow of gas and solid particles is upward in a chamber referred to as the 'riser'. In a CFB, solid particles move upward in the core of the riser and fall downward in the vicinity of the walls, giving much longer solid-residence times than in pneumatic conveying systems. The solid particles which leave the riser are separated in a cyclone and returned to the bottom of the riser. In the last decade or so, CFBs have found application as boilers for power or steam generation in which the fuel is coal or some other sulfur-emitting fuel. In these applications, the solid phase in the reactor is limestone or dolomite (calcium-based solids) which absorbs gaseous sulfur emissions by mixing with the products of combustion. As circulating fluidized-beds become more widely used as boilers, it is important to understand the mechanisms for heat transfer at the walls of CFBs. A means for accurately predicting heat transfer will allow for better designs and more efficient systems.

The heat transfer in a CFB typically takes place on the periphery of the riser with water tubes that comprise the wall of the riser, so that the mechanisms for heat transfer can be described by the interactions between the bed material, the gas and the wall. In a core-annular flow regime, as seen in the upper portion of a CFB, the flow of bed material in an annular region near the wall is predominantly downward in groups of particles known as clusters [1, 2]. The net flow of solids is upward, however, because the cross-section of the annular region is small compared to the core region in which solid particles are flowing upward. Other investigators have found clusters to have the following features: the characteristic size of a cluster, based on the dimension normal to the flow over it, is roughly 0.5–2.0 cm [3, 4]; the typical concentration of solid particles in a cluster is approximately 10–30% [2, 5]; a typical descent velocity is between 0.5 and 2.0 m s^{-1} [3, 6]; and the typical shape projected at the wall is somewhat oval or elliptical [4].

A model for convective heat transfer at the wall of a CFB has been developed by others [5, 7–9] and presented in an earlier work by the authors [10]. In short, the model neglects radiant heat transfer (considering it to be additive) and accounts for the parallel effect of convective heat transfer from the gas phase and transient conduction from the particle phase (also known as particle convection). Based on this model, an expression for the total convective heat-transfer at the wall of a CFB is presented in the following equation:

$$h_{conv} = (1-f)\cdot h_{gas} + f\cdot\left(R_{contact} + \sqrt{\frac{\pi t}{(k\rho c)_{cluster}}}\right)^{-1}. \quad (1)$$

A number of the heat-transfer parameters in equation (1) are functions of the hydrodynamics in a CFB, such as: f, the fraction of the wall covered by clusters; $R_{contact}$, the contact resistance between the cluster and the wall; t, the time of contact between clusters and the wall; and k, ρ and c, the physical properties of the cluster, which are dependent on cluster porosity [11]. Since so much of equation (1) is based on hydrodynamic phenomena, the ability to observe, measure and predict these phenomena under various operating conditions will allow for a better understanding of them and the ability to predict bed-to-wall heat-transfer rates under various operating conditions.

In this work, we are interested in measuring the residence time of clusters at the wall, t, as well as the velocity of these clusters as they travel adjacent to the wall. The motion of the clusters is of particular interest because of the 'renewal' mechanism in the cluster layer. In other words, the heat transfer model is predicated upon the steady deposition and shedding of clusters to and from the wall region. The causes of cluster deposition and shedding at the wall are generally unknown, but in this paper, we attempt to at least explain the mechanism for shedding. This is done by determining the effect that varying operating conditions in the CFB has on these hydrodynamic characteristics, and then using this information to gain insight into the fundamental behavior of the flow of solid particles near the wall of the riser. The development of a technique to measure cluster–wall contact times and cluster descent velocities was reported in a previous paper, and these results were presented for one type of bed material [10]. In this work, the data for cluster velocities and cluster–wall contact times are expanded by varying both the average particle size and material density, as well as the gas superficial velocity and solid recycle rate. Also in another study, a computational flow model capable of solving for flow near permeable bodies, such as the clusters found in a CFB riser, was developed [12]. In this work, the model is extended to include the presence of the riser wall. Results from the model show the existence of lateral lift and vertical drag forces that govern cluster motion at the riser wall and result in the motion of clusters away from the wall (i.e. shedding).

2. Description of experiments

2.1. Scale-model CFB

All the experiments reported here were conducted in a cold-flow scale-model CFB which was originally built as a 1/4-scale model of a 2-MW_{th} combustor [13]. The riser is 2.44 m high with a square cross-section measuring 0.159 m on each side; the walls are made of clear polycarbonate plastic. There are eleven pressure taps along the riser, so that ten differential-pressure measurements are available for the calculation of the average solid-concentration profile in the riser based on the assumption that the pressure drop is equal to the weight per unit area of solid particles suspended in the riser. The riser has a sharp 90° exit at the top, and the solids are returned to the bottom of the bed via an aerated L-valve. Figure 1 shows a schematic of the scale-model CFB.

Three sets of particles were used in these experiments, and they are: steel powder with a material density of 6980 kg m^{-3} and a mean particle size of 69 μm; silica sand with a material density of 2660 kg m^{-3} and a mean particle size of 128 μm; and silica sand with a material density of 2650 kg/m^{-3} and a mean particle size of 182 μm. Particle densities were measured using a helium pycnometer. The distributions of particle sizes were measured by sieving, using a series of stackable trays with screened bottoms of varying fineness, and the mean particle size was calculated based on the average surface-to-volume ratio of the size distribution [14]. Figures 2(a)–(c) present the particle size distributions for each set of particles. Using scale-up rules for CFBs [15], it can be shown that the use of steel allows for the simulation of a larger CFB combustor operating at a pressure of 3.5 atm. Table 1 gives the general specifications of the cold scale-model CFB and the hypothetical full-sized CFBs being simulated by the use of the various particles.

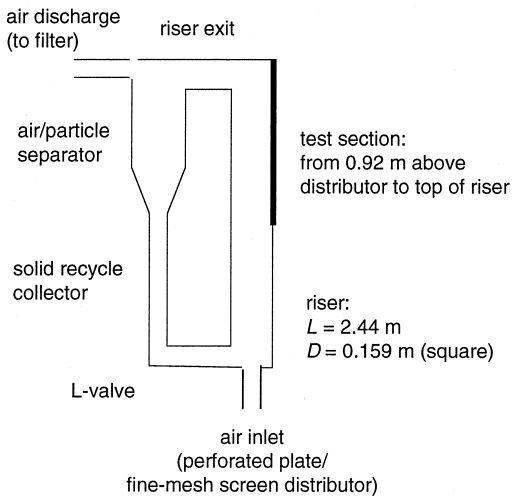

Fig. 1. Schematic for scale-model CFB.

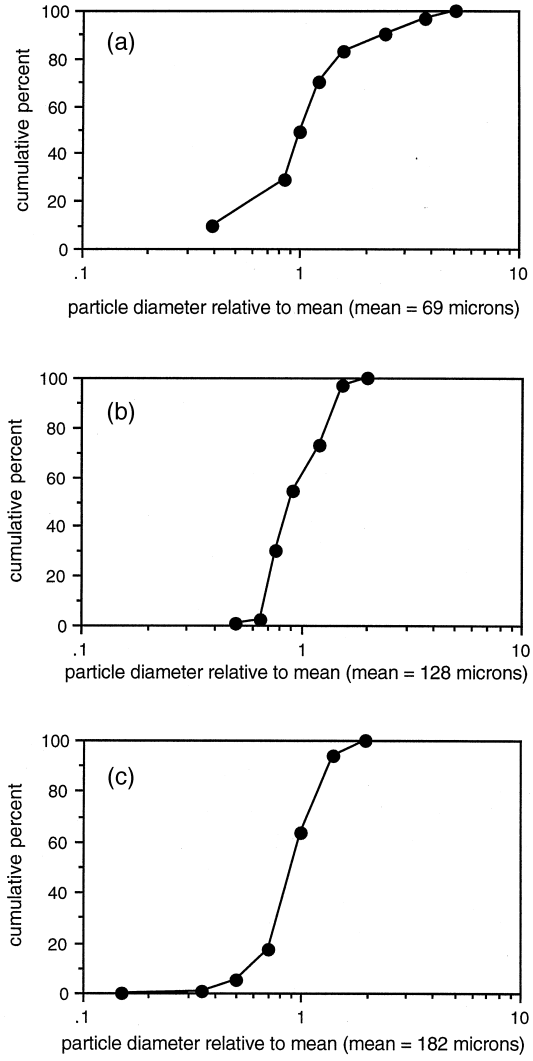

Fig. 2. (a) Particle size distribution for steel powder. (b) Particle size distribution for 128 μm sand. (c) Particle size distribution for 182 μm sand.

2.2. Experimental technique

The technique used to measure both cluster velocities and cluster-wall contact times is called Thermal Image Velocimetry, or TIV. This technique was recently developed by the authors, and a more detailed description can be found in an earlier paper [10]. In short, TIV is a thermal marking technique in which the bed material

Table 1
Specifications for scale-model and hypothetically scaled-up CFBs

Parameter	Scale model w/steel particles	4 : 1 scale-up	Scale model w/sand	4 : 1 scale-up
L (m)	2.44	9.76	2.44	9.76
D (m)	0.159	0.636	0.159	0.636
Cross-section shape	Square	Square	Square	Square
T (K)	300	1100	300	1100
P (atm)	1.0	1.0	1.0	3.5
ρ_g (kg m^{-3})	1.2	0.33	1.2	1.1
ρ_s (kg m^{-3})	6980	$\approx$2500	2660	$\approx$2500
d_p (μm)	69	$\approx$230	128	265
Typical u_0 (m s^{-1})	3	6	3	6
Typical G_s (kg m^{-2} s^{-1})	25	18	15	28

near the wall is heated and the motion is subsequently tracked with an infrared camera. To accomplish this, however, the wall material must be transparent to infrared radiation. A special wall was constructed of low-density polyethylene to meet this requirement. Figure 1 also shows the position of the TIV test section in the scale-model CFB. TIV has several advantages: it is a non-invasive method for marking the clusters and tracking their motion at the wall, as no instrumentation is required in the flow path; and it does not require the addition of tracer particles to the flow to enhance flow visualization, which is beneficial since such particles might affect the hydrodynamics in the riser. The simple method of marking the clusters with heat does not require a special bed material (such as photo-luminescent substance). This allows the selection of a material which will yield similitude with any desired full-sized configuration.

2.3. Experimental operating conditions

The scale-model CFB was run at a total of sixteen different operating conditions for these experiments. Eight of these were with the steel particles, six were with the 128 μm sand and two were with the 182 μm sand. By changing the bed material, we were able to observe variations in cluster-wall contact with both solid density and particle size (or minimum fluidization velocity, alternatively). It should be noted that the steel and the 128 μm sand can be shown to have approximately the same minimum fluidization velocity—1.2 cm s^{-1} for the steel, and 1.6 cm s^{-1} for the 128 μm sand [14]. The gas superficial velocity and solid recycle rate were varied in order to understand the effect of these operating conditions on wall hydrodynamics. When possible, attempts were made to match u_0 and G_s on both a dimensional and a dimensionless basis between experiments with different solid particles, in which the dimensionless gas velocity is given by u_0/u_{mf} and the dimensionless solid recycle rate is given by $G_s/(\rho_s u_0)$. Table 2 lists the operating conditions along with the average local solid concentrations in the test section. The average local solid concentrations were calculated by measuring the local pressure drop along the riser and equating that to the weight of solids suspended in that region.

3. Experimental results

3.1. Overview

With the TIV technique, clusters of particles are heated as they pass into the test section and the infrared camera

Table 2
Experimental operating conditions and results

Bed material	u_0 (m s^{-1})	G_s (kg m^{-2} s^{-1})	Avg. local solid conc. (%)	Avg. total contact time (s)
Steel	2.3	9.3	0.25	0.49
	2.8	11	0.21	0.37
	2.8	19	0.46	0.45
	2.7	30	0.56	0.37
	3.3	18	0.24	0.37
	3.3	28	0.42	0.42
	3.6	25	0.28	0.38
	3.6	34	0.49	0.33
128 μm	2.5	13	0.63	0.22
sand	2.5	21	0.89	0.24
	2.9	11	0.51	0.31
	3.2	14	0.46	0.20
	3.3	18	0.54	0.21
	1.8	11	0.90	0.14
182 μm	2.9	15	0.75	0.40
sand	3.4	15	0.61	0.28

can be focused at different elevations for a certain period of time. Analyzing the resulting videotape in slow motion yields both the velocities of the clusters via measurement of distance traveled over elapsed time, as well as a probability distribution function for cluster presence at the wall. The decay of this probability function can be shown to be equal to the probability function for cluster motion away from the wall, and the average of the subsequent probability function has been shown to be one-half the average cluster-wall contact time [16]. Since the detection of clusters depends on their temperature, it may be possible that the disappearance of clusters results from cooling; however, it has been shown that the heater has enough power to sufficiently raise the temperature of almost all of the clusters such that they can be observed, or such that they have not cooled down, by the end of the entire test section [17]. This ensures that the measured changes in the passing frequency are due to clusters moving away from the wall, and not from clusters cooling down. Details of this technique are discussed in a previous paper [10].

3.2. Measurements of cluster descent velocities

Cluster velocities at the wall of the riser were measured under the operating conditions listed in Table 2. The uncertainty error associated with the velocity measurements is roughly $\pm 30\%$ [10]. The average cluster velocity measured in all the cases was between 1.1–1.2 m s^{-1}. These values are roughly independent of variations in operating conditions: gas superficial velocity, solid recycle rate, solid density and average particle diameter. Our observations are roughly consistent with results that have been widely reported which show that cluster velocities at the wall of a CFB are typically on the order of 1 m s^{-1} [17]. We may be missing some of the smaller variations, however, since the relatively poor resolution of the measurement system for measuring cluster velocities results in a relatively large error.

3.3. Measurements of cluster–wall contact times

The residence times of clusters at the wall of the riser were also measured under the operating conditions listed in Table 2. The total uncertainty of the measured distribution function of contact times from the infrared videotape is about $\pm 15\%$. The measured velocities are used in reducing the video data for contact times, so that a root-mean-square method for combining these uncertainties [18] yields a total uncertainty for contact times of about $\pm 35\%$ [10].

Figures 3–6 show how the cluster–wall contact times vary with the gas superficial velocity, the solid recycle rate, the average local cross-sectional solid concentration (equivalent to G_s), the solid density and the average particle diameter. As with the velocity measurements, the experimental uncertainty may hide some trends. However, there appears to be no dependence of contact time on superficial velocity, solid recycle rate or the local cross-sectional void fraction (see Figs 3–5). Figure 6 shows that there is a fairly direct correlation between contact time and solid density, as well as with average particle size for the same density. It seems somewhat intuitive that larger or heavier particles will be more difficult to move away from the wall and clusters of these particles will therefore have longer residence times.

3.4. Relating cluster–wall contact to heat transfer

One way to evaluate the impact of the observed differences in cluster–wall contact times is to use them in conjunction with the model presented in equation (1) to calculate bed-to-wall heat-transfer coefficients. This model requires knowledge of several other hydrodynamic parameters, but estimates for these can be made based on previous research [5]: $f \approx 0.50$, $h_{gas} \approx 12$ W m^{-2} K^{-1}, $R_{contact} \approx 0.0024$ m^2 K^{-1} W^{-1}, and $\sqrt{(k\rho c)_{cluster}} \approx 100$ m^2 K^{-1} W^{-1} $s^{-1/2}$. For the contact times measured, one can estimate that use of the lighter particles might results in nearly a 30% increase in heat transfer when compared to the heavier particles. This seems to indicate that a CFB running at elevated pressure, in which the particles are lighter relative to the gas, will have higher heat transfer rates; higher heat transfer rates in pressurized CFBs vs. atmospheric CFBs have been observed in some instances [19]. However, the heat transfer model for CFBs requires knowledge of other hydrodynamic parameters, such as the fractional wall coverage by clusters and the cluster–wall contact resistance, which are likely to change with operating pressure and therefore make it difficult to conclusively compare the relative merits of pressurized or atmospheric CFBs for heat transfer.

4. Modeling the cluster–wall interaction

4.1. Motivation

Given the observations and measurements of cluster motion near the wall in a CFB, we now turn our attention to an explanation of the observed behavior. One clue for an explanation is in the dependence of cluster–wall contact time on the inertia of individual particles. Particles of larger diameter and denser materials tend to have longer contact times. To a first approximation, then, one could assume that clusters of these particles would also be heavier, leading to more inertia and greater resistance to forces that might be controlling the near-wall motion of the clusters. These concepts led us to investigate the aerodynamic forces acting on a cluster resulting from the relative motion between the cluster, the wall and the gas flowing in the CFB. To simplify the model, the gas flow

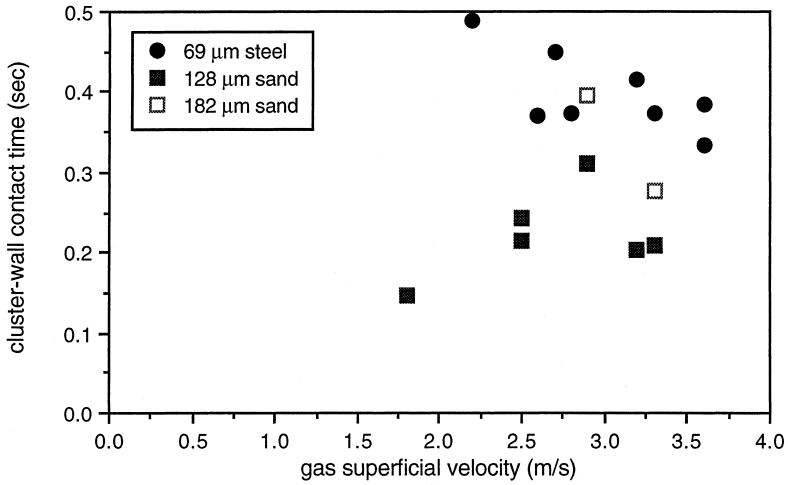

Fig. 3. Cluster–wall contact time vs gas superficial velocity.

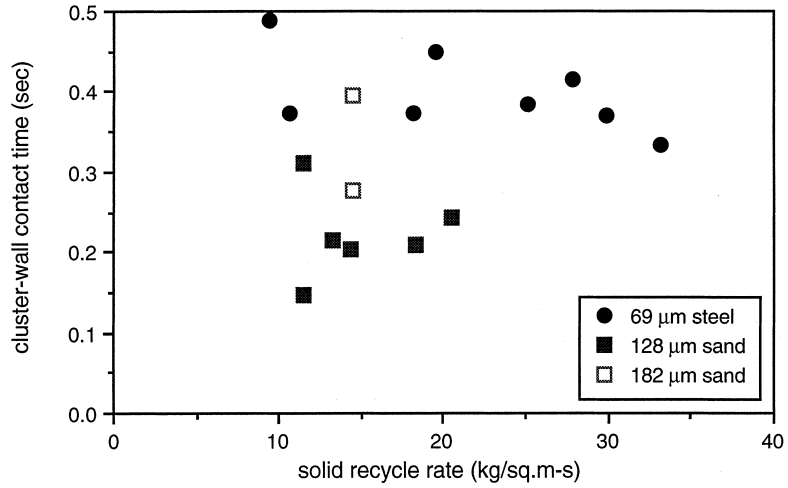

Fig. 4. Cluster–wall contact time vs solid recycle rate.

near the wall can be neglected. Rashidi et al. [20] found that particle-laden flows exhibited delayed boundary layer growth away from the wall, creating a larger zone of low gas momentum near the wall. This phenomenon also appears in our results, in that the cluster descent velocity is apparently independent of the superficial gas velocity. This indicates that the gas velocity can be neglected for the purposes of simplifying this modeling process.

4.2. Background

There does not appear to be any previous work under exactly the same flow conditions studied here; namely, no one has ever studied the flow past a permeable body moving relative to a stationary wall in a quiescent fluid. There are, however, studies of flow past permeable bodies and flow past solid bodies near walls, but not both. Most of the previous studies have been conducted at relatively low Reynolds numbers, where the Reynolds number is defined as the product of the velocity of the body and the diameter of the body divided by the kinematic viscosity of the surrounding fluid. For clusters of particles in a CFB, a typical Reynolds number might be on the order of 1000, using 1 m s^{-1} for a typical descent velocity, 1 cm for a typical cluster length scale [3, 21], and 10^{-5} as an order-of-magnitude value for the kinematic viscosity of the ambient air in a cold-flow CFB.

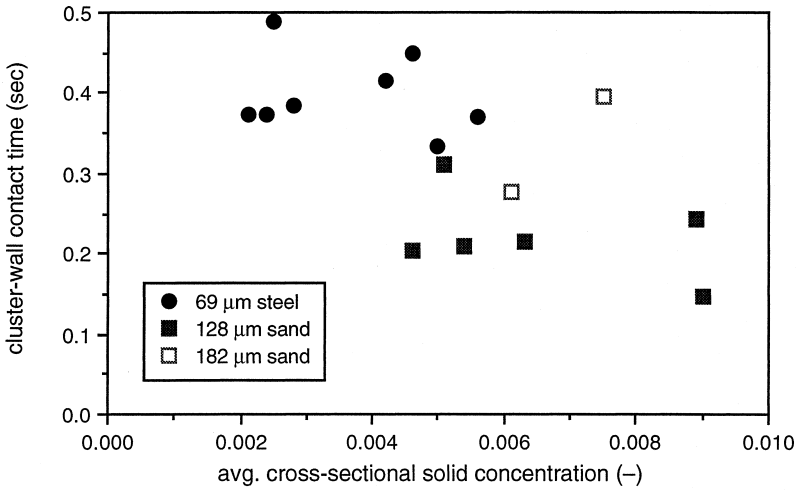

Fig. 5. Cluster–wall contact time vs solid concentration.

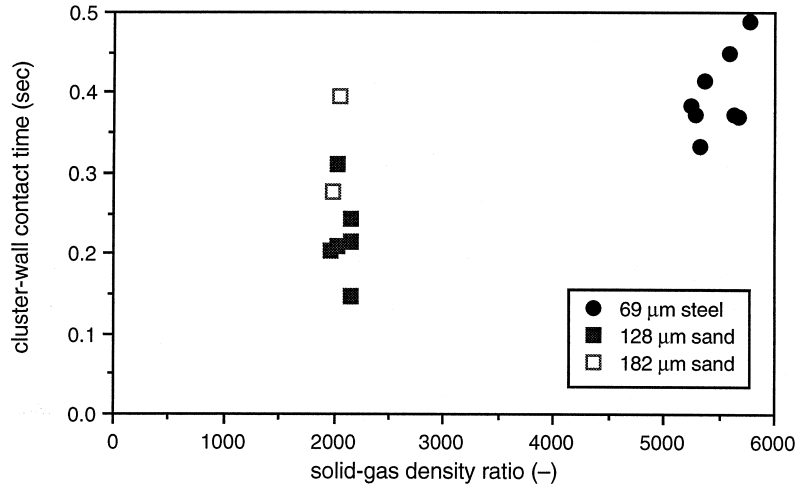

Fig. 6. Cluster–wall contact time vs solid–gas density ratio.

Goldman et al. [22] showed that the motion of a sphere near a wall in a quiescent fluid can increase drag by a factor of about five, with the augmentation of drag depending on distance from the wall. Saffman [23] showed that a sphere in the boundary layer of a viscous flow near a wall will experience a force directed away from the wall, or a lifting force. Both of these results are for 'vanishingly small' Reynolds numbers, and therefore potentially lack applicability to the current configuration. At the other end of the Reynolds number spectrum, Carr [24] tested scale models of automobiles in a wind tunnel with $Re > 10^5$ and with a conveyor belt to simulate relative motion between the automobile and the ground. Carr's results show that the proximity of the body to the ground can either increase or decrease drag, depending on the shape of the body. Similarly inconclusive results were compiled by Hucho [25], although it appears that drag and lift tend to increase with decreasing ground clearance for automobiles with increasing underbody convexity.

These previous results say nothing conclusive about cluster motion at moderate Reynolds numbers, but they indicate that the presence of the wall should have an effect, and that lift and drag might both increase with proximity to the wall if the cross-section of the cluster is considered to be convex or simply round. As a result of the lack of directly applicable work, we developed a computational model to study the hydrodynamic forces acting on a cluster moving near the wall in a CFB.

4.3. Description of CFD model

A commercially-available program for computational fluid dynamics (CFD) was used in this study. The CFD program is PHOENICS, Version 2.1.1, produced by CHAM Ltd [26]. PHOENICS employs finite-volume methods for the solution of the governing equations for fluid dynamics, and provides as output the pressure and velocity fields on the user-specified discrete computational domain. Internal to PHOENICS are some built-in functions to assist in computations for more complex flows, accounting for the effects of turbulence or permeability, for example. The use of these is discussed later.

For simplicity and to make the problem tractable, a cluster is modeled as a permeable cylinder—a round, two-dimensional object with no relative motion among the particles within the cluster. Although the results from such a model will not be exactly applicable to clusters in a CFB, the results will indicate the presence and significance of forces acting on a permeable body moving near a wall. Figure 7 gives a schematic of the model and the pertinent nomenclature. The computational domain is a Cartesian coordinate system that is distorted into a round shape in the region of the cylinder. In this study, the origin of the coordinate system has been defined at the point on the cylinder that is closest to the wall. The computational domain and the discretized elements are shown in Fig. 8. The domain extends three cylinder diameters upstream of the windward face of the cylinder, 10 diameters downstream of the leeward face of the cylinder, and 5 diameters above the top-most point on the cylinder. The gap between the cylinder and the wall is one of the parameters to be varied in this study. One hundred elements comprise the cylinder itself, for which the permeability can be varied. The size and fineness of the computational domain were determined after conducting a variational study in order to verify accuracy and convergence of solutions. A similar computational model was used to study the drag on permeable cylinders relative to solid cylinders in unbounded flow at similar Reynolds numbers [12].

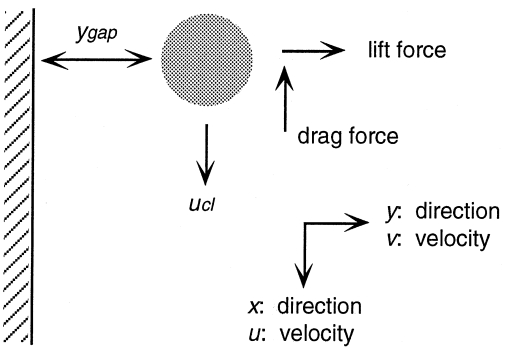

Fig. 7. Schematic of computational model.

Within the permeable cylinder, mass conservation and D'Arcy's Law for flow in a permeable body are applied in order to solve for the pressure and velocity fields. The mass conservation equation for two-dimensional, incompressible flow is given by the following expression [27]:

$$\nabla \cdot \mathbf{v} = 0 \tag{2}$$

and the conservation of momentum is expressed in D'Arcy's Law [28]:

$$\nabla P = \frac{\mu \mathbf{v}}{\kappa} \tag{3}$$

A modification to D'Arcy's Law established by Brinkman [29] is a more general statement of momentum conservation for the inner region. However, an order-of-magnitude analysis shows that Brinkman's formulation reduces to equation (3) when the ratio of permeability and the square of the system length scale is less than unity. In subsequent sections, we define this ratio as the 'permeability ratio' and in this study, the permeability ratios considered are generally orders of magnitude smaller than unity. As a result, we believe that equations (2) and (3) adequately describe the flow field within the porous cylinder without Brinkman's modification.

Outside of the permeable cylinder, the mass conservation expression of equation (2) is applied, while the two-dimensional, incompressible form of the Navier–Stokes equation is used to solve for the momentum of the fluid flow [27]:

$$\rho \mathbf{v} \cdot \nabla \mathbf{v} = -\nabla P + \mu \nabla^2 \mathbf{v}. \tag{4}$$

The solutions for pressure and flow are matched at the interface of the two regions, and the boundary conditions that are specified are the ambient pressure on the exterior of the domain and the cluster velocity on the exterior of the domain to the windward side of the cylindrical body. Matching the mass flow of the outer region to that of the inner region at the interface between the two provides the second boundary condition for velocity required by equation (4). In addition to the boundary conditions already specified, the wall is defined as a solid surface moving at the same velocity as the incoming air (i.e. the air is quiescent relative to the wall and in motion relative to the cluster). No initial conditions are required since the flow is considered steady.

The effects of turbulence were ignored for the purposes of this study. PHOENICS has a variety of self-contained turbulence of the 'k–epsilon' type. The use of these models at the Reynolds numbers in question only affected the results for drag coefficient on a solid cylinder by about 0.1%; this was not deemed sufficient to warrant the added computational time (approximately double when including turbulence) or complexity [12]. This is likely due to the fact that turbulence does not play a significant role

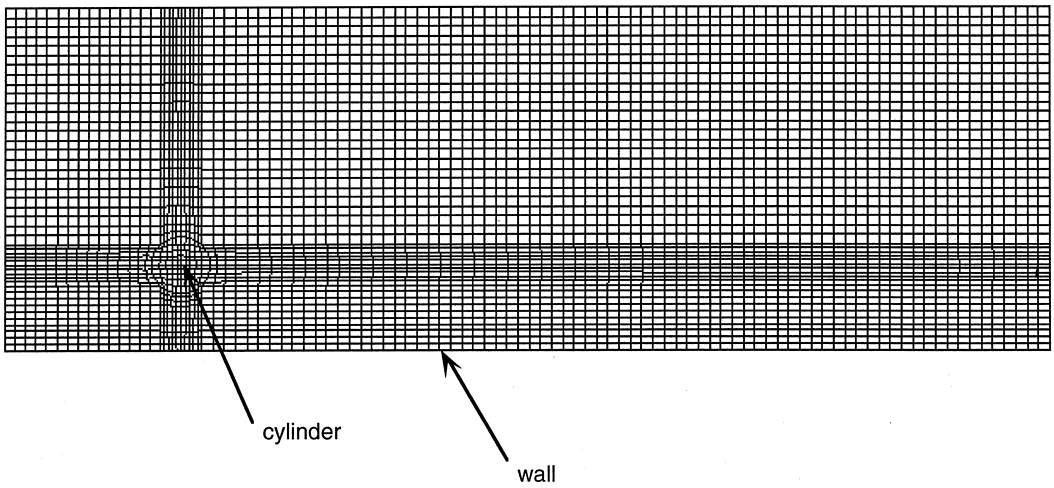

Fig. 8. Computational domain for motion of a cylinder (cluster) near a wall.

in the boundary layer on a cylinder for $Re < 10\,000$; the conditions studied here represent $10 \leqslant Re \leqslant 1000$.

As a final word on the computational methods, some discussion of the 'post-processing' of the raw output is warranted. As mentioned previously, the PHOENICS output consists of the pressure and velocity fields in each discretized element. A linear momentum balance on a control volume away from the cylinder surface yields the following expression for the net force on the body as a function of the change in momentum of the fluid passing through the control volume and the net pressure force on the control volume:

$$F_i = \int_A P\,\mathrm{d}A_i - \int_A \rho v_i \mathbf{v}\cdot\mathrm{d}\mathbf{A} \tag{5}$$

where i represents one of the directions and A_i represents the area per unit length of cylinder projected in the ith direction. In the x-direction, $F_i = F_x$ is the drag force, while in the y-direction, $F_i = F_y$ is the lifting force. Given either component of the force on the cylinder, the drag and lift coefficients can be calculated from their definitions for a cylindrical body [25]:

$$c_\mathrm{d} = \frac{F_x}{\frac{1}{2}\rho u^2 D} \quad \text{and} \quad c_\mathrm{l} = \frac{F_y}{\frac{1}{2}\rho u^2 D} \tag{6}$$

where u is the free-stream velocity in the model (the velocity of the cluster), and D is the diameter of the cylindrical body.

5. Results of modeling and comparison to experiments

5.1. Results of CFD modeling

There are three independent dimensionless parameters in this study: the Reynolds number based on the diameter of the cylinder; the ratio of the permeability, κ, to the square of the cylinder diameter, D, which is inversely related to the solid fraction of a cluster [30]; and the 'gap ratio', or the ratio of the gap between the cylinder and the wall to the cylinder diameter. The gap ratio is represented by the symbol $y_* = y/D$. For brevity, a parametric study was run for only a select number of conditions. Figures 9–14 present the lift and drag coefficients for the geometry of Figs 7 and 8 as a function of permeability ratio for $Re = 10$, 100 and 1000 and $y_* = 0.10$, 0.01 and 0.001. These values were chosen as representative values found in CFBs, and lift and drag were computed for permeability ratios between 10^{-5} and 10^{-3} for the same reason. The drag coefficients are presented as 'drag ratios', or the ratio of the computed drag coefficient to that for an equivalent solid cylinder in an unbounded flow field. The drag coefficient for a solid cylinder in an unbounded flow field varies with Reynolds number; computed values for these can be found in a previous paper [12] or empirical values can be found in textbooks [31].

The results show that the drag on a permeable cylinder near a wall increases by a factor of two to three compared to a solid cylinder far from a wall, and the increase in drag increases with proximity to the wall. Similarly, there is an appreciable lift coefficient that also increases as the gap ratio decreases. Depending on the speed, gap size and permeability, the lift coefficient is roughly 0.5–1.5. Both the lift coefficient and the drag ratio approach free-stream values, as expected, as y_* increases, and similar trends with permeability ratio are seen with cylinders in unbounded flow [12]. Interestingly enough, there is little change in either lift or drag from $y_* = 0.01$ to $y_* = 0.001$. This is likely due to the fact that such a small gap creates a flow resistance of similar magnitude to the permeable body itself. As the gap size decreases, the flow

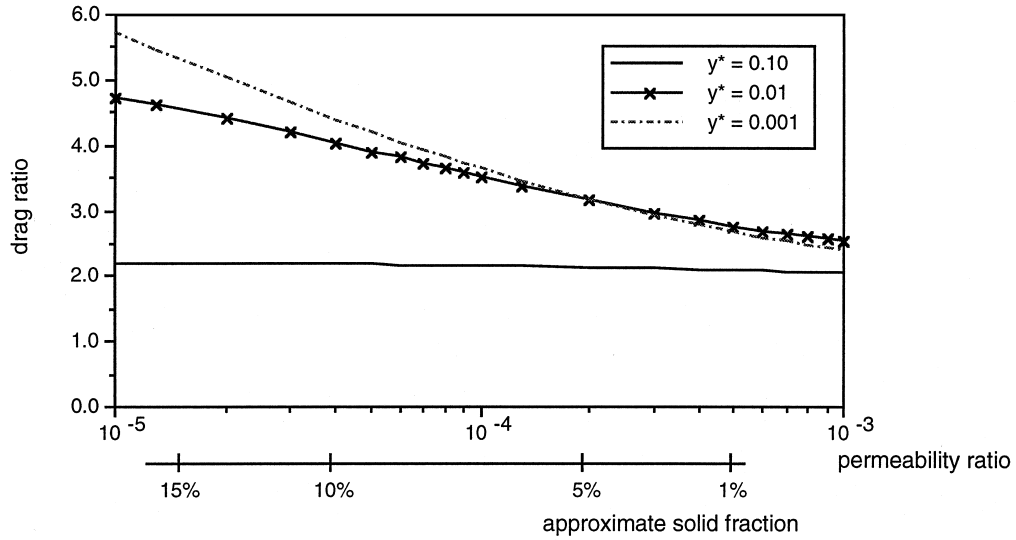

Fig. 9. Drag ratio vs permeability ratio, $Re = 10$.

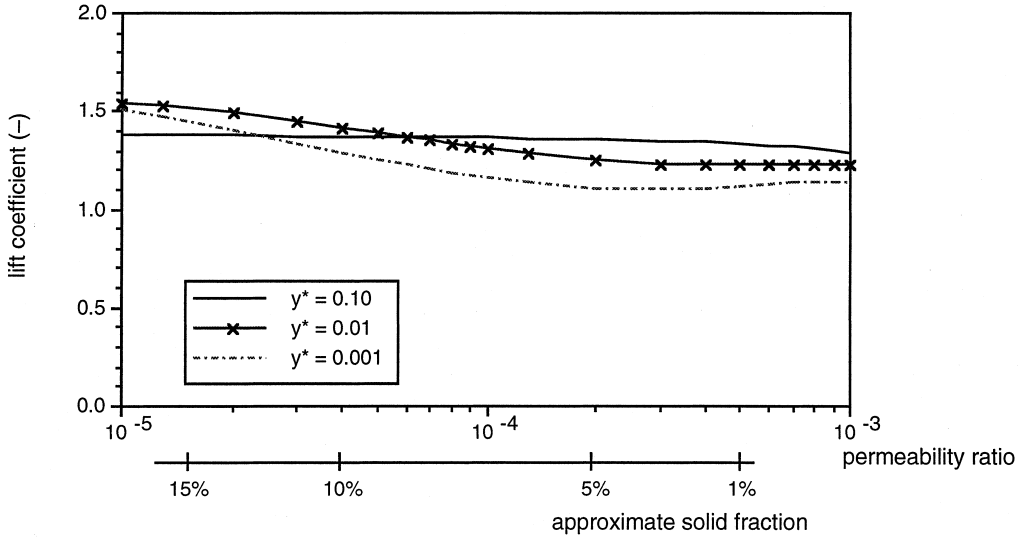

Fig. 10. Lift coefficient vs permeability ratio, $Re = 10$.

resistance in the gap may increase but that region becomes negligible relative to the permeable cylindrical region and therefore has a negligible effect on the overall results. The presence of this lifting force also helps explain the existence of the contact gap between the cluster and the wall which was measured by Lints and Glicksman [5].

5.2. Comparison of drag results to measured cluster velocities

Simple aerodynamic drag calculations for a solid body of similar size and weight far from a wall tend to over-predict the terminal velocity of a cluster by a factor of about three (when using the typical value of 10% for the solid fraction in the cluster [5]). This indicates that such a simple analysis under-predicts the actual drag force by a factor of roughly 10. Given the results from the computational model, it appears that the combination of permeability and wall proximity only double or triple the drag relative to the simple aerodynamic drag. It should be noted, though, that the many simplifications in this model can contribute to this shortfall. For example, neglecting the upward gas flow opposing the cluster, strictly speaking, is not correct. Given typical cluster

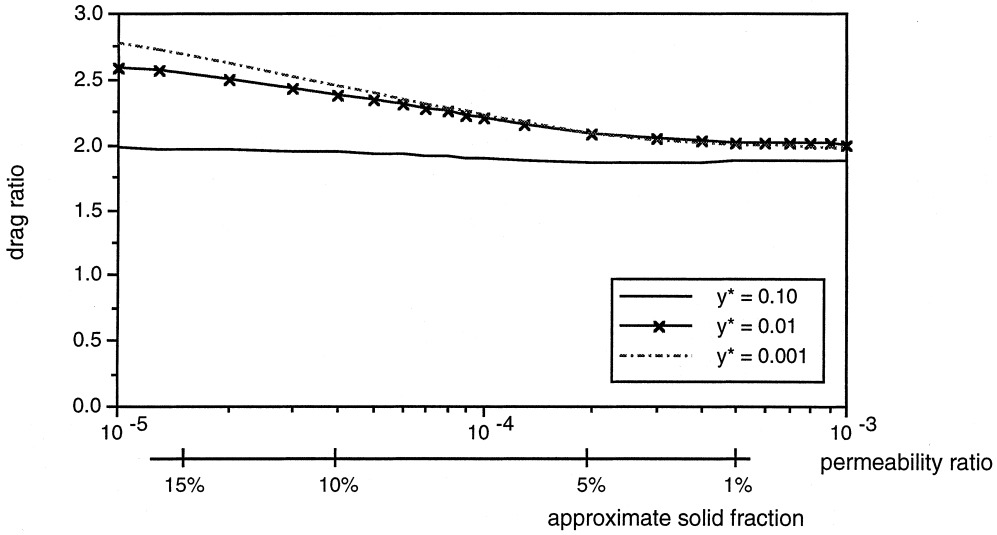

Fig. 11. Drag ratio vs permeability ratio, $Re = 100$.

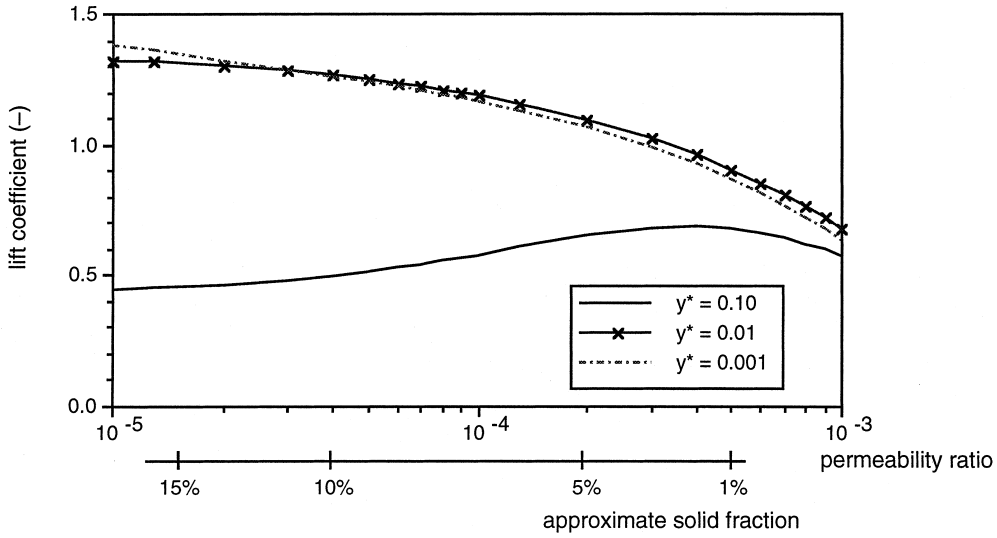

Fig. 12. Lift coefficient vs permeability ratio, $Re = 100$.

sizes and distances from the wall, the gas velocity in the boundary layer might be 10–50% of the gas superficial velocity in the CFB based on single-phase calculations. This represents a substantial velocity opposing the motion of the cluster and would create a significant increase in the drag force on a cluster. However, the applicability of single-phase boundary layer calculations to gas–particle flows are suspect, and the gas flow in the wall region is expected to be lower in a CFB. Also, the shape of the cluster is not necessarily regular. Analysis by Lim et al. [4] suggests that considering an elliptical shape for a cluster can double the drag coefficient in unbounded flow relative to a round body, while Potter and Foss [32] present similar results for objects of square cross-section. Simply applied to the present results for drag near a wall, this would suggest a four- or six-fold increase in drag which begins to approach the increase required to explain the observed velocities. The fact that there is a net drag force on the cluster of particles also implies that a cluster will deform and not be round or even have a constant cross-sectional shape. The effect of shape factor is also likely to be different when considering the presence of the wall, however, and this may increase the drag ratios even further.

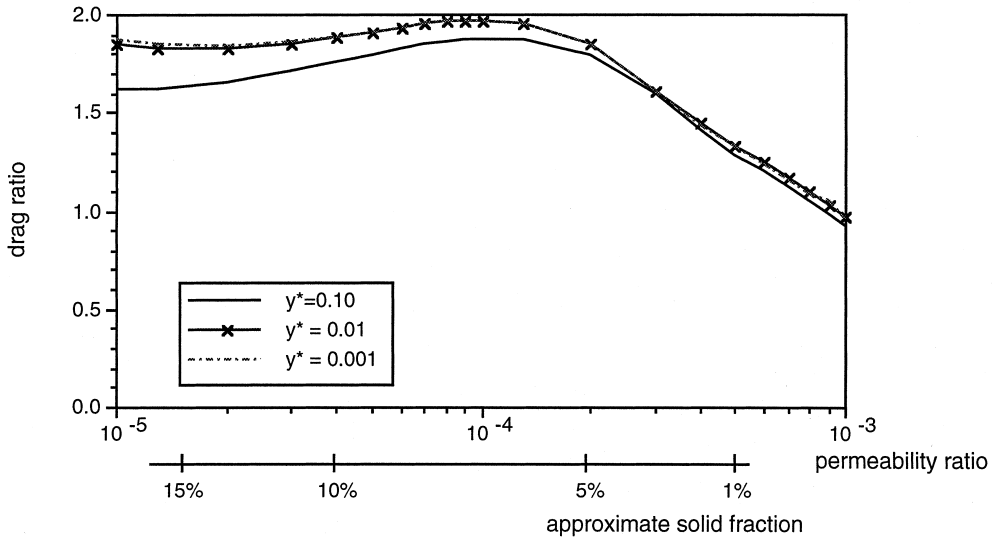

Fig. 13. Drag ratio vs permeability ratio, $Re = 1000$.

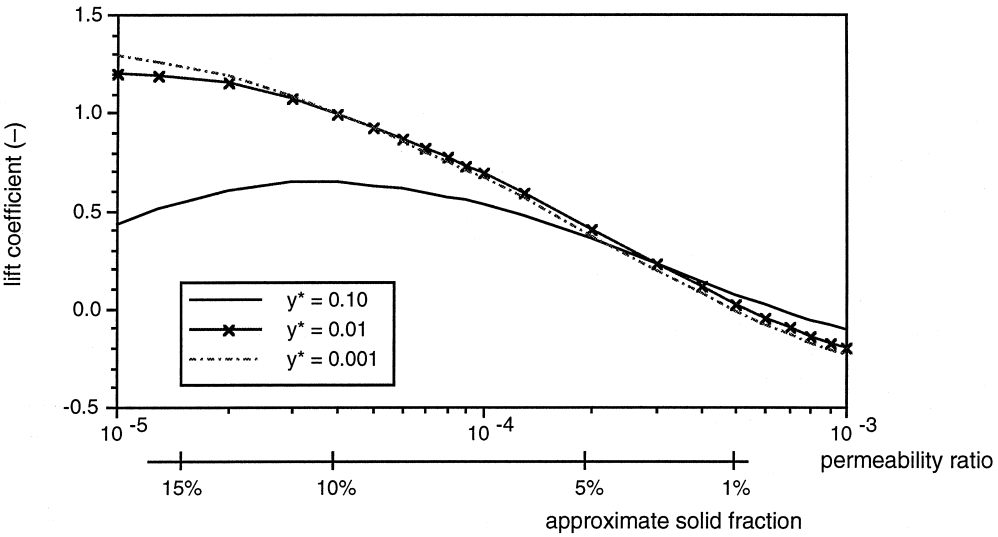

Fig. 14. Lift coefficient vs permeability ratio, $Re = 1000$.

5.3. Comparison of lift results to measured cluster–wall contact times

The laws of motion can be used to apply the computed lift and drag coefficients toward understanding the cluster–wall contact interaction. Force balances on the cluster in both the vertical (x)- and lateral (y)-directions can be written as follows:

$$\Sigma F_x = m_{\mathrm{cl}} x'' = m_{\mathrm{cl}} g - c_{\mathrm{d}} \frac{1}{2} \rho_{\mathrm{g}} (x')^2 D_{\mathrm{cl}} \tag{7}$$

$$\Sigma F_y = m_{\mathrm{cl}} y'' = c_{\mathrm{l}} \frac{1}{2} \rho_{\mathrm{g}} (x')^2 D_{\mathrm{cl}} \tag{8}$$

where m_{cl} represents the mass per unit length of the cylindrical body and the superscripts $'$ and $''$ represent the first and second derivatives with respect to time. From these equations, the following differential equations can be written to describe the motion of a cylindrical cluster:

$$x'' = g - \frac{2}{\pi} \frac{c_{\mathrm{d}} \rho_{\mathrm{g}} (x')^2}{\rho_{\mathrm{s}} (1 - \varepsilon_{\mathrm{cl}}) D_{\mathrm{cl}}} \tag{9}$$

$$y'' = \frac{2}{\pi}\frac{c_l \rho_g (x')^2}{\rho_s (1-\varepsilon_{cl}) D_{cl}} \tag{10}$$

In equations (7)–(10), the added mass terms have been neglected since $\rho_s \gg \rho_g$. Solutions of these equations for $x(t)$ and $y(t)$ are clearly difficult—equations (9) and (10) are coupled, and they are both non-linear with non-constant coefficients (both c_d and c_l vary with x' and y). With a few simple assumptions, however, a solution can be generated for comparison to the CFB experiments.

First, consider that the cluster velocity is nearly constant as a function of time, at a value of 1 m s^{-1} perhaps. This results in a constant value for the lift coefficient as well, say about 0.5 judging from the results presented in Fig. 12. Assuming the other parameters to be constant and assuming initial values $y(0) = y'(0) = 0$, equation (10) can be integrated to yield:

$$y(t) = \frac{1}{\pi}\frac{c_l u_{cl}^2 t^2}{\rho_* (1-\varepsilon_{cl}) D_{cl}}. \tag{11}$$

Furthermore, it can be argued that at some critical distance y_{cr} from the wall, the cluster will either be far enough from the wall to have a negligible contribution to heat transfer, or it will stray into a region of high enough gas velocity to be dragged upward with the core flow. Based on heat transfer arguments, a cluster–wall gap of 5 mm results in a thermal resistance similar in magnitude to that from gas convection in a CFB; it can also be shown that 5 mm is about the thickness of the viscous sub-layer of the turbulent boundary layer if calculated based on single-phase gas flow. Taking $y_{cr} = 5$ mm, then, a solution for the time to reach y_{cr} can be obtained from equation (11):

$$t = \sqrt{\frac{y_{cr}\rho_* (1-\varepsilon_{cl}) \pi D_{cl}}{c_l u_{cl}^2}}. \tag{12}$$

Values for the other parameters can be estimated: $\rho_* \approx 6000$ as with steel particles, $\varepsilon_{cl} \approx 90\%$, $D_{cl} \approx 1$ cm, $c_l \approx 0.5$. Substituting these values into equation (12) yields $t \approx 0.4$ s, which is bout the same as the average measurements for steel. It is gratifying that such a simple analysis can be used to predict the contact time within an order of magnitude, especially considering the uncertainty of the values for ε_{cl} and D_{cl} as well as the approximations made to linearize the differential equation. In fact, the most important point that can be drawn from equation (12) is this: the contact time predicted varies with $\sqrt{\rho_*}$, which is the trend observed in the experimental data taken in the CFB. For a factor of 2.6 variation in ρ_*, a factor of about 1.8 variation in t was observed; equation (12) predicts a factor of 1.6 variation in t for the same variation in ρ_*. This agreement is extremely close and it lends credence to the hypothesis that the lift force on the cluster governs the cluster–wall contact time. Figure 15 presents the magnitude and trends for contact times predicted by equation (12) superimposed upon the experimental results.

This analysis can be further refined by integrating equation (11) while accounting for the variation in lift coefficient with distance from the wall. Figure 16 presents the computational results and curve fit for lift coefficient as a function of distance for a 1 cm cylinder with a 10% solid fraction moving at 1 m s^{-1} in room temperature air. The functional form of the curve fit is $c_l = 0.35 - 0.29\log(y/D_{cl})$. Since lift varies with the square of velocity, it can be assumed that the lifting force is very

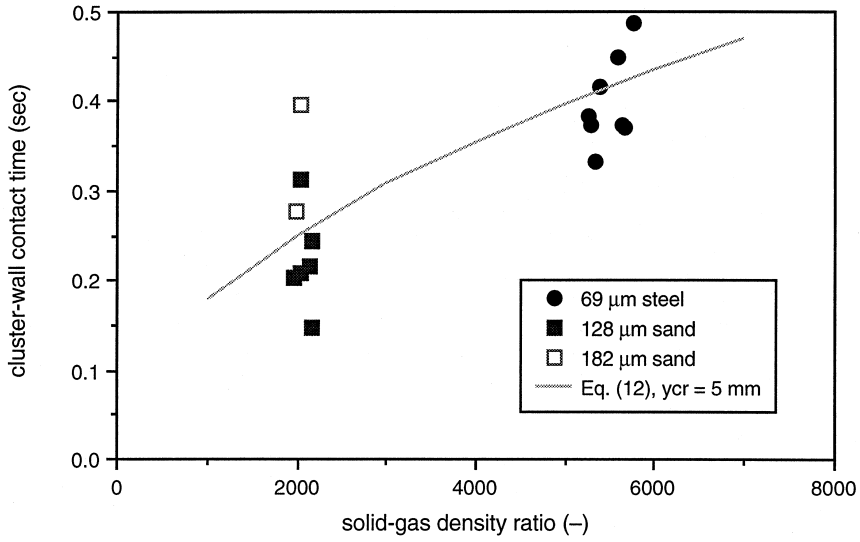

Fig. 15. Application of lift-model predictions to experimental results.

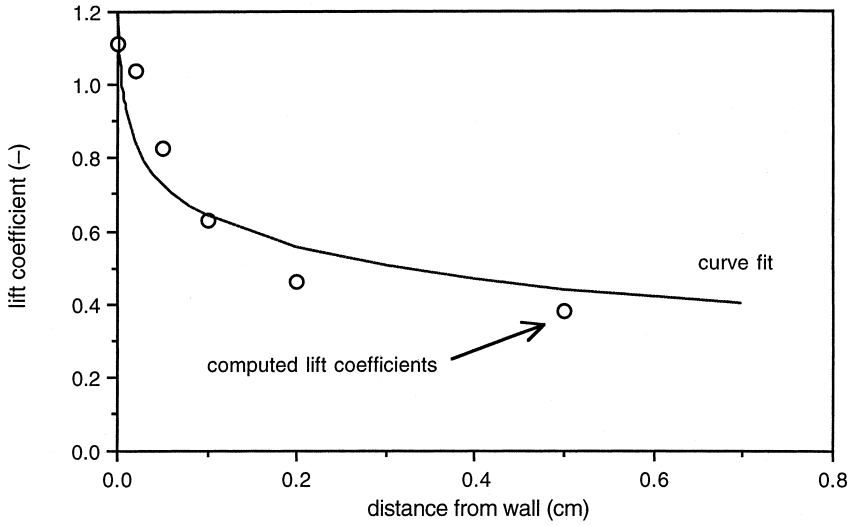

Fig. 16. Lift coefficient vs distance from wall.

small at low velocities and that most of the lifting force occurs near the maximum velocity. This allows for the assumption that the $(x')^2$ term in equation (11) is nearly constant. With this and the functional form of c_l, equation (11) can be numerically integrated to yield a similar result as before—showing that it takes 0.36 s for the cylinder to travel 5 mm laterally. This level of analysis retains the dependence of contact time on the square-root of solid density seen in Fig. 15.

6. Conclusions

In a cold scale-model CFB, a relatively new experimental technique was used to measure the residence times and velocities of clusters at the wall of a CFB. It was found that for a smooth-walled CFB of square cross-section, the cluster velocities are between 1.1–1.2 m s^{-1}, with no apparent variation with operating conditions. These results are consistent with previously reported cluster velocities. Cluster–wall contact times were also measured in the range of 0.15–0.50 s, with a dependence on solid density observed. In modeling the motion of a cluster adjacent to the CFB wall as a permeable body moving in a quiescent fluid near a solid boundary, computational methods were employed to study the horizontal (lift) and vertical (drag) forces on the body. This analysis showed that the presence of the wall results in a lifting force on the cluster, which helps to explain the observed shedding of clusters from the wall region in a CFB. Analysis of the motion of a cluster in the presence of the lifting force predicts the magnitude and trends observed for cluster–wall contact times. This lends credence to the hypothesis that these near-wall hydrodynamic forces contribute substantially to the motion of clusters at the wall and also to heat transfer in a CFB, for which cluster motion is an important parameter.

Acknowledgements

This work was sponsored by the National Science Foundation. The authors are grateful to the Welding Laboratory and the Fluid Mechanics Laboratory at MIT for the use of their equipment, and to Professor Qingyan Chen and Weiran Xu of MIT for their guidance in the use of the CFD software.

References

[1] H. Ishii, T. Nakajima, M. Horio, The clustering annular flow model of circulating fluidized beds, Journal of Chemical Engineering of Japan 22 (1989) 484–490.
[2] C.H. Soong, K. Tuzla, J.C. Chen, Identification of particle clusters in circulating fluidized beds, in: A. Avidan (Ed.), Circulating Fluidized Bed Technology IV, 1993 pp. 615–620.
[3] M. Rhodes, H. Mineo, T. Hirama, Particle motion at the wall of a circulating fluidized bed, Powder Technology 70 (1992) 207–214.
[4] K.S. Lim, J. Zhou, C. Finley, J.R. Grace, C.J. Lim, C.M.H. Brereton, Cluster descending velocity at the wall of circulating fluidized bed risers, 5th International Conference on Circulating Fluidized Beds, Beijing, P.R.C., 1996.
[5] M.C. Lints, L.R. Glicksman, Parameters governing particle-to-wall heat transfer in a circulating fluidized bed, in: A. Avidan (Ed,), Circulating Fluidized Bed Technology IV, 1993, 297–304.

[6] T. Wang, Z.J. Lin, C.M. Zhu, D.C. Liu, S.C. Saxena, Particle velocity measurements in a circulating fluidized bed, AIChE Journal 39 (1993) 1406–1410.
[7] D. Subbaro, P. Basu, A model for heat transfer in circulating fluidized beds, International Journal of Heat and Mass Transfer 29 (1986) 487–489.
[8] H.S. Mickley, D.F. Fairbanks, Mechanism of heat transfer to fluidized beds, AIChE Journal 1 (1955) 374–384.
[9] A.P.Baskakov, The mechanism of heat transfer between a fluidized bed and a surface, International Chemical Engineering 4 (1964) 320–324.
[10] P.D. Noymer, L.R. Glicksman, Cluster motion and particle-convective heat transfer at the wall of a circulating fluidized bed, International Journal of Heat and Mass Transfer 41 (1998) 147–158.
[11] N.I. Gelperin, V.G. Einstein, Heat transfer in fluidized beds. In: J.F. Davidson, D. Harrison (Eds.), Fluidization, Chap. 10, Academic Press, 1971.
[12] P.D. Noymer, L.R. Glicksman, A. Devendran, Drag on a permeable cylinder in steady flow at moderate Reynolds numbers, Chemical Engineering Science 53 (1998) 2859–2869.
[13] D. Westphalen, Scaling and lateral solid mixing in circulating fluidized beds, Ph.D. thesis, Massachusetts Institute of Technology, Cambridge, MA, 1993.
[14] J.R. Grace, Fluidized-bed hydrodynamics. In: G. Hetsroni (Ed.), Handbook of Multiphase Systems, Chap. 8, Hemisphere Publishing, 1982.
[15] L.R. Glicksman, M. Hyre, K. Woloshun, Simplified scaling relationships for fluidized beds, Powder Technology 77 (1993) 177–199.
[16] S.B. Panta, A probabilistic analysis for the interpretation of flow-visualization data at the wall of a circulating fluidized bed, B.S. thesis, Massachusetts Institute of Technology, Cambridge, MA, 1996.
[17] P.D. Noymer, Heat transfer by particle convection at the wall of a circulating fluidized-bed, Ph.D. thesis, Massachusetts Institute of Technology, Cambridge, MA, 1997.
[18] T.G. Beckwith, R.D. Marangoni, J.H. Lienhard V, Mechanical Measurements, 5th ed., Chap. 3, Addison-Wesley, 1993.
[19] P. Basu, L. Cheng, K. Cen, Heat transfer in a pressurized circulating fluidized bed, International Journal of Heat and Mass Transfer 39 (1996) 2711–2722.
[20] M. Rashidi, G. Hestroni, S. Banerjee, Particle–turbulence interaction in a boundary layer, International Journal of Multiphase Flow 16 (1990) 935–949.
[21] B. Zou, H. Li, Y. Xia, X. Ma, Cluster structure in a circulating fluidized bed, Powder Technology 78 (1994) 173–178.
[22] A.J. Goldman, R.G. Cox, H. Brenner, Slow viscous motion of a sphere parallel to a plane wall—I: motion through a quiescent fluid, Chemical Engineering Science 22 (1967) 637–651.
[23] P.G. Saffman, The lift on a small sphere in a slow shear flow, Journal of Fluid Mechanics 22 (1965) 385–400.
[24] G.W. Carr, A comparison of the ground-plane-suction and moving-belt ground-representation techniques, Paper No. 880249, Society of Automotive Engineers, Warrendale, PA, 1988.
[25] W.-H. Hucho (Ed.), Aerodynamic drag of passenger cars, in: Aerodynamics of Road Vehicles, Chap. 4, Butterworths, 1987.
[26] Concentration, Heat and Momentum, Ltd., PHOENICS Users Manual, London, 1991.
[27] F.M. White, Viscous Fluid Flow, 2nd ed., McGraw-Hill, 1991, pp. 61–69.
[28] A.E. Scheidegger, The Physics of Flow through Porous Media, University of Toronto Press, 1960, pp. 69–71.
[29] H.C. Brinkman, A calculation of the viscous force exerted by a flowing fluid on a dense swarm of particles, Applied Scientific Research A 1 (1947) 27–34.
[30] A.E. Scheidegger, The Physics of Flow through Porous Media, University of Toronto Press, 1960, p. 129.
[31] F.M. White, Viscous Fluid Flow, 2nd ed., McGraw-Hill, 1991, pp. 181–184.
[32] M.C. Potter, J.F. Foss, Fluid Mechanics, Great Lakes Press, 1982.